Int J Adv Manuf Technol (2017) 90:1605–1615
DOI 10.1007/s00170-016-9465-8

ORIGINAL ARTICLE

An investigation into the behavior of the cutting forces in precision turning

M . A. Shalaby [1] · M. A. El Hakim [2] · S. C. Veldhuis [1] · G. K. Dosbaeva [1]

Received: 10 May 2016 / Accepted: 8 September 2016 / Published online: 28 September 2016

Abstract A mechanistic model of precision turning, in which the depth of the cut is made considerably smaller than the tool nose radius, based on Merchant's analysis in 3D cutting, has been developed. Reasons were deduced to the increase of the radial force component to be greater than the tangential component. The friction coefficient at the tool chip interface during precision turning has been calculated. The developed model was verified experimentally using both annealed and hardened HSS. Moreover, due to the obsoleteness of empirical formulae established by previous investigators in the case of precision turning, new empirical formulae based on the mechanistic model are presented. In this machining operation, the behavior of the cutting forces in relation to the cutting variables, revealed their high sensitivity to tool nose radius and flank wear land width.

Keywords Precision turning · Mechanistic model · Empirical model

Nomenclatures

a	Depth of cut
VB	Tool flank wear land width
b_1, b_2	Undeformed and deformed chip width, respectively
F_a	Axial force component
F_c	Main cutting force component
F_{ch}	Component of force along tool face
F_f	Friction force
F_n	The component of force normal to the tool face
F_r	Radial force component
F_s	The component of force along shear plane
h_1, h_2	Undeformed and deformed chip thickness, respectively
h_{av}	Average undefomed chip thickness
MFTW	Machine-fixture-tool-workpiece
r	Tool nose radius
s	Feed
v	Cutting speed
α	Clearance angle
γ	True rake angle
γ_n	Normal rake angle
γ_x	Side rake angle
γ_y	Back rake angle
δ_s	Angle that the shear force makes with normal to the cutting edge in this plane
λ_c	Chip compression ratio
φ_c	Contact angle
χ	Plan approach angle
χ_e	Effective lead angle
μ	Friction coefficient at the tool-chip interface

1 Introduction

In precision turning, considerably small values of depth of cut and feed are used together with large nose radius to achieve the assigned surface quality and dimensional accuracy. It was widely accepted for cylindrical grinding to be replaced, due to its economical and ecological benefits [1, 2]. As well, the turned surfaces may have a longer fatigue life when compared with ground ones [3, 4].

✉ G. K. Dosbaeva
jdosby@mcmaster.ca

[1] McMaster University, 1280 Main St. West, Hamilton, ON L8S 4L7, Canada

[2] Faculty of Engineering, Ain Shams University, Cairo, Egypt

When the cutting edge nose radius is remarkably greater than the depth of cut, it was found that the cutting force components increase by increasing the cutting edge radius. This increase of the cutting forces can be associated with the change of the frictional conditions between the tool and the workpiece contact [5]. During precision turning, researchers observed that the radial cutting force is usually the largest component [1, 6–9].

Significant advances were achieved in experimental study and modeling of cutting forces in different machining processes [10, 11]. The effect of the cutting conditions on the cutting force components in hard precision machining has been presented by many researchers [12–15]. Afazov et al. [5] investigated the effect of process variables on cutting force components in micro-milling. Qian et al. [10] carried out numerical simulation of hard turning. The modeling of static and dynamic cutting forces has also been discussed [16]. A link between plasticity parameters and cutting conditions has been established by Agrnell et al. [17].

In spite of the presented extensive work, the reason behind increasing the radial cutting force component during precision turning greater than tangential and axial components still needs more clarification.

Due to large tool radius when compared with the depth of cut, and low feed used in precision turning, the calculation method for the undeformed chip thickness in conventional turning is not suitable. The calculation of the undeformed chip thickness during precision turning would enhance the understanding of the process as a result [18].

When a continuous chip is formed in machining, it remains in contact with the tool rake face over certain distance known as tool-chip contact length, which plays an important role in metal cutting process; it affects the cutting force and temperature. Two regions exist in a whole tool chip contact length; the first is the sticking zone close to the tool edge followed by the sliding zone. Experiments with different materials and cutting conditions showed that the tool-chip contact length is related to the chip compression ratio (λ_c), which is defined as the ratio between the deformed chip thickness (h_2) to the undeformed chip thickness (h_1). It is usually used as an indication of the frictional condition on the tool face [19].

The increase of flank wear results in larger plastic zone in the tertiary deformation zone and hence increases the cutting force components [20].

Mechanistic and empirical models have been used to perform modeling of the cutting process due to their great importance for industrial applications [21–23]. Empirical modeling of the cutting force can be considered the simplest approach [24]. It can be used for predicting the cutting force components in machining processes, which is necessary for design, selection, and purchase of machine tools. The tangential force component (F_c) and the feed force component (F_a) are needed to calculate the torque and the power of the main and feed drives, respectively. The radial force component (F_r) is responsible for the Machine-Fixture-Tool-Workpiece (MFTW) system deflections and hence the workpiece dimensional errors [25]. It is used to determine the depth of cut for the assigned dimensional accuracy, which is essential in precision turning [7, 26, 27].

The empirical relationships have been established by previous investigators between the cutting force components and the cutting variables; the depth of cut (a) and the feed (s) were found to be only applicable when the a is larger than the nose radius (r). No formula has yet been obtained for precision turning where (a/r) << 1.

The objective of present research is to establish a mechanistic model explaining why an increase of the radial force component is greater than the tangential component in precision turning. It can also be used to find the effect of the ratio of the a to the r on the ratio between the F_r and the F_c. The suggested model will be utilized to predict the coefficient of friction at the tool-chip interface (μ), which is used to explain many phenomena encountered during precision turning such as tool wear and cutting temperature [28]. In this study, chip compression ratio has been used as an indication of the frictional conditions at the tool-chip interface at different cutting speeds. Undeformed chip thickness during precision turning was calculated in this work.

Empirical formulae which relate the cutting force components to the machining variables in precision turning were established. The effects of the tool nose radius and tool flank wear land width on the cutting force components are included in the empirical equations.

2 Experimental work

AISI T1e5 high-speed steel (HSS) has been chosen as the workpiece material during the present study. Machining tests were carried out in on both the annealed (28 HRC) and hardened (52 HRC) states of the workpiece material. The latter hardness value is usually used for deep drawing, punching and extrusion dies. A MAS 3 kW digitally controlled general purpose centre lathe has been used. The maximum error in the machine tool slides is 10 μm for the maximum distance between centers (1500 mm). A KISTLER 3-component tool force turning dynamometer has been used for measuring the three cutting force components. The error of the measured cutting force components using the dynamometer is within ±0.1 %. To reduce the effect of tool wear on the cutting force results, the cutting force measurements have been obtained using tool inserts having a flank wear land width not exceeding 0.05 mm, except when investigating the effect of tool wear on the cutting force components. The calibration of the cutting forces dynamometer was carried out using a loading device with a capacity of 2000 N. Calibration was repeated three times and the average least squares calibration line has been

used. The produced chips were collected at different speeds and their thicknesses were measured using a digital micrometer with 10 μm resolution to determine the λ_c.

A MITUTOYO tool maker's microscope with 1 μm resolution was used to measure the tool flank wear land width (VB). Tool life was determined at 0.2 mm flank wear. A multi-coated carbide tool has been used to machine the annealed and hardened workpieces as it demonstrated good performance in cutting the same material [29]. The used cutting variables are illustrated in Table 1.

3 The mechanistic model

There is an urgent need to move from 2D to 3D models in machining operations. Most fundamental variables and machining performance measures are predicted in 2D, whereas industry requires 3D modeling [10]. A 3D oblique cutting model was used by many other researchers in thread cutting [30], end milling [31], and also extrapolated from a 2D model [32].

However, precision turning will be carried out using a r to attain the required surface finish. The a will be necessarily smaller than the nose radius, Merchant's method for oblique cutting is proposed for the establishment of the mechanistic model as shown in Fig. 1a.

The assumptions of this model are the same as those of the original Merchant's model [33]; the tool starts sharp and remains sharp until the end of cutting, the shear zone is approximated to a plane, continuous chip is obtained without BUE, the chip does not move laterally, and the cutting speed is uniform. These assumptions have so far been fulfilled as permitted by turning practice.

Figure 1b illustrates the contact angle (φ_c) between the cutting tool and machined surface, given by:

$$\phi_c = \cos^{-1}\left(\frac{r-a}{a}\right) \tag{1}$$

Table 1 Cutting parameters

Cutting conditions	Range
Cutting speed (v)	40–275 m/min
Feed range (s)	0.025–0.1 mm/rev
Depth of cut range (a)	0.07–0.27 mm
Tool nose radius (r)	0.4–1.6 mm
Tool holder specifications	−6° rake angle, −3° side rake angle, and −9° back rake angle, +5° clearance angle
Time of cutting force measurement	10–15 s, depending on the cutting speed and feed
Time of engagement during cutting force measurement	7–10 s, depending on the cutting speed and feed

As shown in Fig. 1b, the undeformed chip thickness (h_i) varies from (0) at $\varphi_i = 0$ to (h_{max}) at $\varphi_i = \varphi_c$.

So that, the average undeformed chip thickness (h_{av}) is given by:

$$h_{av} = \frac{1}{\phi_c}\int_0^{\phi} h_i \mathrm{d}\phi \tag{2}$$

Substituting with $h_i = s \sin\varphi_i$ in Eq. (1), the h_{av} is given by:

$$h_{av} = \frac{1}{\phi_c}\int_0^{\phi} s\sin\phi_i \mathrm{d}\phi = -\frac{s}{\phi_c}[\cos\phi]_0^{\phi_c} = \frac{s}{\phi_c}(1-\cos\phi_c) \tag{3}$$

Substituting with $\phi_c = \cos^{-1}\left(\frac{r-a}{a}\right)$ in Eq. (3), the undeformed chip thickness (h_1) is given by:

$$h_1 = h_{av} =^{\text{av}} \frac{sa}{r\phi_c} \tag{4}$$

The undeformed chip width (b_1) is a direct function of the r and the φ_c (Fig. 1b):

$$b_1 = r\phi_c = r\sqrt{\frac{2a}{r}} = \sqrt{2ar} \tag{5}$$

Accordingly, it can be deduced that:

$$b_1 \propto a^{0.5} r^{0.5} \tag{6}$$

The plan approach angle (χ) varies from point-to point along the r, starting from zero at the beginning of the φ_c at the end of contact (Fig. 1b). So that for a small arc of contact, an average χ is taken as follows:

$$\chi = 0.5\phi_c \tag{7}$$

The inclination angle (λ), presented in Fig.1a, is the angle between the cutting edge and the normal to the cutting velocity vector ($\vec{v}$) in a plane containing ($\vec{v}$) and the cutting edge. It can be expressed as a function of the back rake angle (γ_y), the side rake angle (γ_x), and the χ as follows [34]:

$$\tan\lambda = \tan\gamma_y \sin\chi - \tan\gamma_x \cos\chi \tag{8}$$

The normal rake angle (γ_n) is the angle measured from a plane normal to the cutting velocity ($\vec{v}$) in a plane perpendicular to the cutting edge to the tool rake face as illustrated in Fig.1a. The true rake angle (γ) is the angle measured from a plane normal to the cutting velocity ($\vec{v}$) to the tool face in a plane containing the cutting velocity vector. The γ_n can be readily expressed in terms of the γ as follows:

$$\tan\gamma_n = \tan\gamma\cos\lambda \tag{9}$$

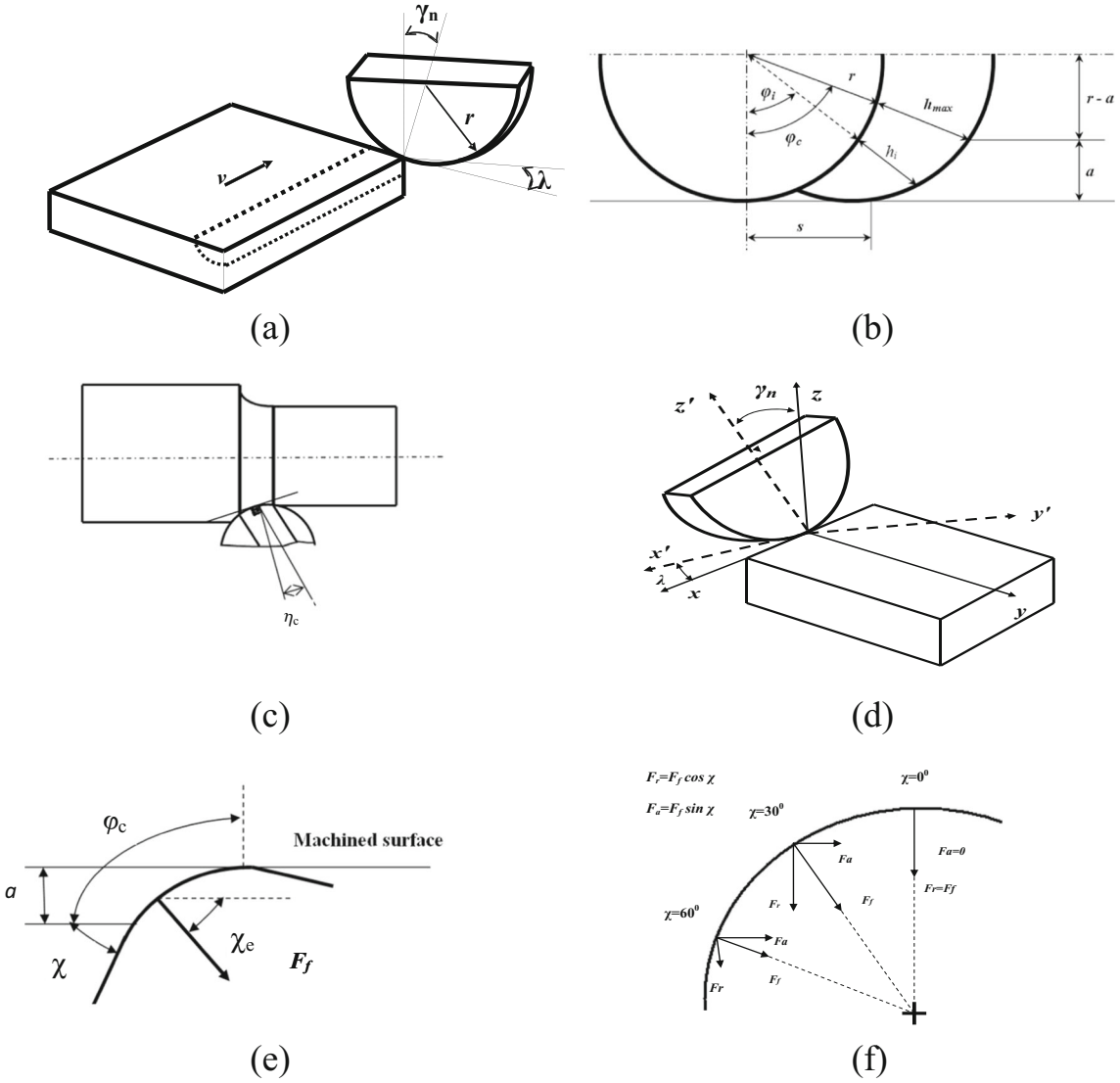

Fig. 1 Proposed Merchant's method for oblique cutting for the establishment of the mechanistic model

The chip flow direction (η_c) is the angle between the chip flow direction and the normal to the cutting edge (Fig. 1c), given by:

$$\cos\eta_c = \frac{b_2}{b_1}\cos\lambda \tag{10}$$

Where (b_2) is the deformed chip width. For small λ, $b_2 \approx b_1$, and $\eta_c \approx \lambda$ [36].

In order to evaluate a three-dimensional cutting operation, it is necessary to determine the mutually perpendicular components of the resultant cutting force. The measured components will be along x- (axial), y- (tangential), and z-axis (radial) of the workpiece. To calculate the components of the cutting force in the plane of the tool face, the coordinates will be changed to x', y', z'; where (x') is along the cutting edge that is tangent to the tool nose arc, (y') is normal to the tool face, and (z') is normal to the cutting edge (in the radial direction of the tool nose arc) (Fig. 1d). The transformation can be readily expressed as follows; considering the force components acting on the cutting tool [33]:

$$F_{x'} = -x_1 F_a - y_1 F_c \tag{11}$$

$$F_{y'} = -x_2 F^2{}_a - y_2 F_c + {}^c z_2 F_r \tag{12}$$

$$F_{z'} = -x_3 F_a - {}^a y_3 F_c + z_3 F_r \tag{13}$$

Where the direction cosines are given by:

$x_1 = \cos\lambda, y_1 = -\sin\lambda, x_2 = \cos\gamma_n \sin\lambda, y_2 = \cos\gamma_n \cos\lambda, z_2 = \sin\gamma_n,$
$x_3 = -\sin\gamma_n \sin\lambda, y_3 = -\sin\gamma_n \cos\lambda, z_3 = \cos\gamma_n$

The component of force along the tool face (F_{ch}):

$$F_{\mathrm{ch}} = \sqrt{F_{x'}{}^2 + F_{z'}{}^2} \tag{14}$$

The angle (δ_c) that the force along the plane of tool face (F_{ch}) makes with the normal to the cutting edge in this plane:

$$\tan\delta_c = \frac{F_{x'}}{F_{z'}} \tag{15}$$

The angle (ζ_c), which is the difference between (η_c) and (δ_c):

$$\zeta_c = \eta_c - \delta_c \tag{16}$$

The friction force (F_f):

$$F_f = F_{ch}\cos\zeta_c \tag{17}$$

The component of force normal to the tool face (F_n):

$$F_n = F_{y'} \tag{18}$$

The μ: is given by the force tangential to the tool face (F_f) divided by the normal force (F_n).

$$\mu = \frac{F_f}{F_n} \tag{19}$$

A flow chart to calculate the μ is presented in Fig 2.

Cutting force values can be obtained by relating them to the cutting pressure on the tool face (k_n), the uncut chip area (A_1), the μ, and the effective lead angle (χ_e). The effective lead angle determines the direction of the friction force as presented in Fig. 1e. When the depth of cut is less than the nose radius ($a << r$), χ_e is determined as follows [34]:

$$\tan\chi_e = 0.5053\cot\chi + 1.0473\left(\frac{s}{r}\right) + 0.4659\left(\frac{r}{a}\right) \tag{20}$$

The cutting force components are computed as follows:

The F_c:

$$F_c = k_n A_1\left(\cos\gamma_y\cos\gamma + \mu\left(\cos\chi_e\sin\gamma + \sin\chi_e\sin\gamma_y\right)\right) \tag{21}$$

The F_a:

$$F_a = k_n A_1\left(-\cos\gamma_y\sin\gamma + \mu(\sin\chi_e\cos\gamma)\right) \tag{22}$$

The F_r:

$$F_r = k_n A_1\left(-\sin\gamma_y + \mu\left(\sin\chi_e\cos\gamma_y\right)\right) \tag{23}$$

$$A_1 = b_1 h_1 = r h_1 \phi_c \tag{24}$$

$$k_n = \frac{F_n}{A_1} = \frac{F_{y'}}{A_1} \tag{25}$$

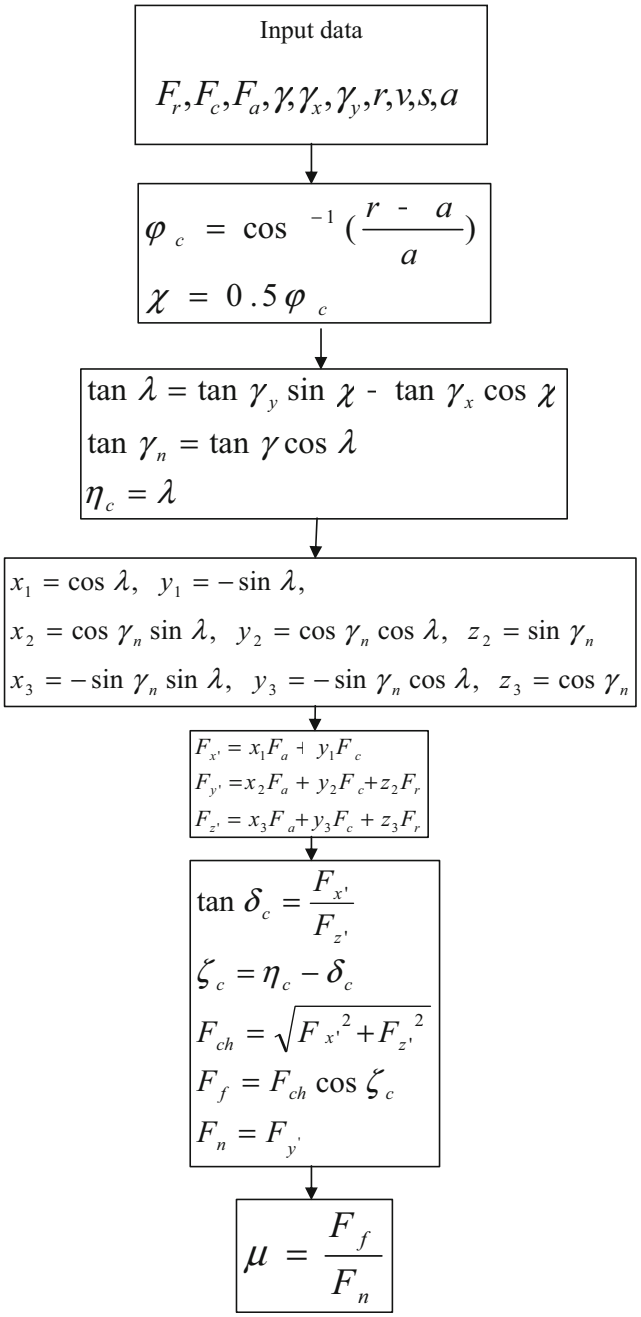

Fig. 2 Flow chart used to calculate the coefficient of friction (μ)

By dividing F_r by F_c:

$$\frac{F_r}{F_c} = \frac{\left(-\sin\gamma_y + \mu\left(\sin\chi_e\cos\gamma_y\right)\right)}{\cos\gamma_y\cos\gamma + \mu\left(\cos\chi_e\sin\gamma + \sin\chi_e\sin\gamma_y\right)} \tag{26}$$

Figure 3 shows the flow chart used to calculate the ratio of the radial force component to the tangential force component (F_r/F_c).

In precision turning, the a is taken <0.1 mm while the r is >0.4 mm for the sake of higher workpiece accuracy and hence $a << r$, which results in the following effects described below.

Figure 1f presents a schematic of the effect of the r on the χ. Figure 4 shows the effect of the r on the χ for different values of the a as deduced from Eq. (7). It can be easily deduced that the increase of the nose radius and/or the decrease of the depth of cut decreases the approach angle, which increases the F_r.

The effect of the a on the ratio F_r/F_c for different nose radii is presented in Fig.5a. F_r/F_c increases as the a decreases for the same nose radius. The effect of the r on the ratio F_r/F_c for different values of the depth of cut is shown in Fig. 5b. F_r/F_c increases as the r increases for the same a.

The increase of F_r/F_c to be ≥1 is caused by the increase of the μ at the tool-chip interface to be ≥0.73 (Fig. 6).

The effect of the a on the value of the χ_e for different nose radii is presented in Fig. 7a. It is apparent that as the a decreases, the χ_e increases until it approaches 90°, which means that the friction force will be more directed towards the radial direction of the workpiece, which causes the resultant cutting force to approach the direction of the radial cutting force. Figure 7b shows the effect of the r on the value of the χ_e for different values of the depth of cut. It can be seen that the χ_e increases with the increase of the r for the same a, which directs the friction force towards the radial direction. This causes the resultant cutting force to approach the direction of the radial cutting force.

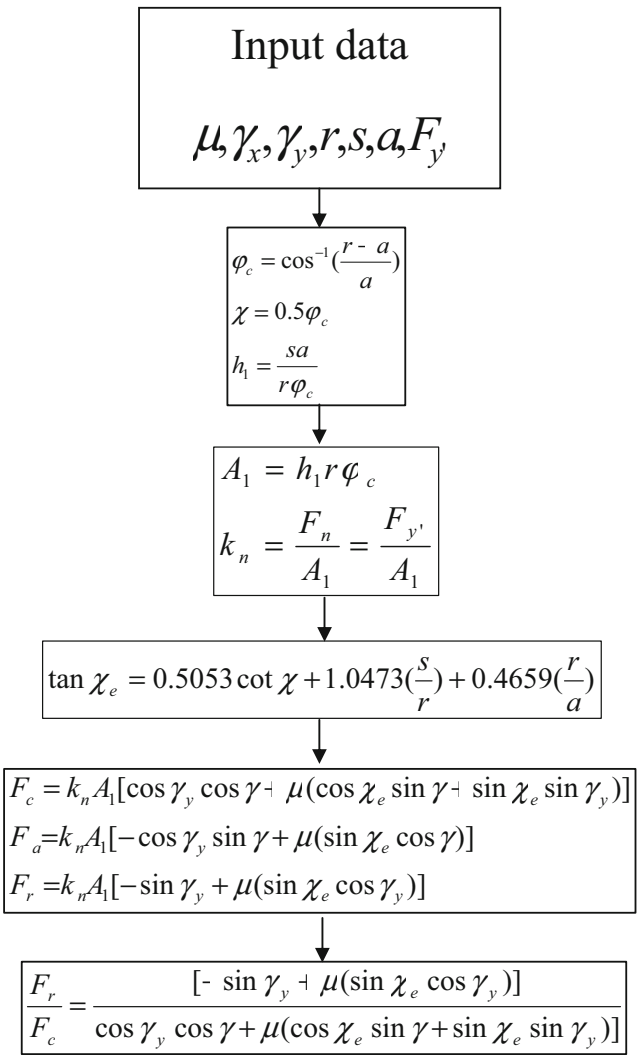

Fig. 3 Flow chart used to calculate the ratio of the radial force component to the tangential force component (F_r/F_c)

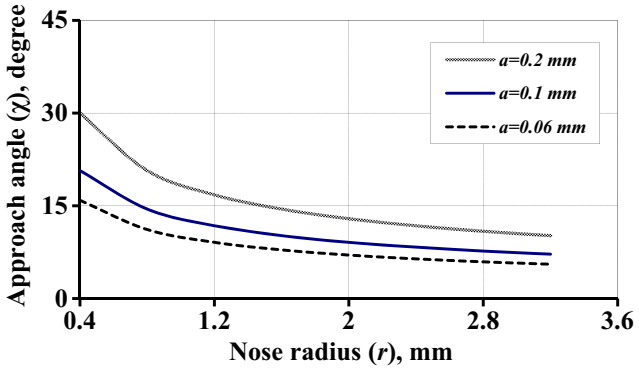

Fig. 4 Effect of the nose radius (r) on the approach angle (χ) for different values of the depth of cut (a)

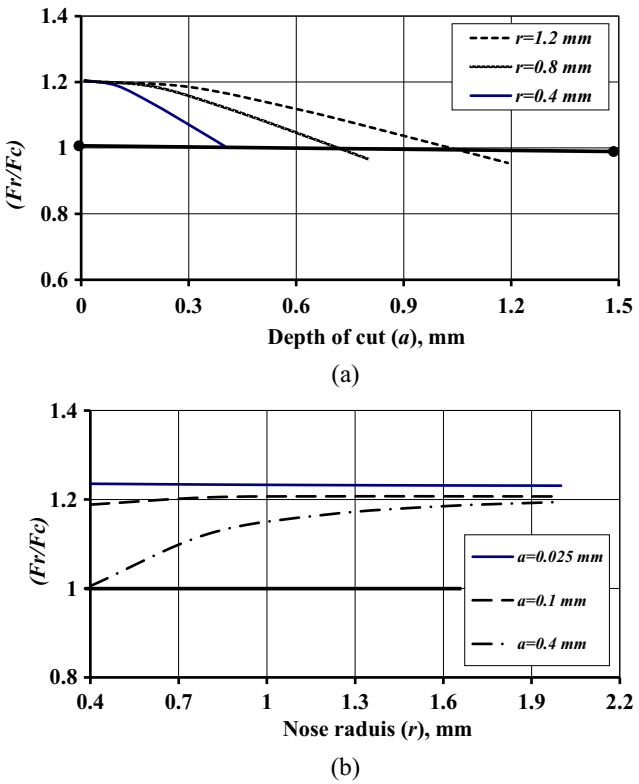

Fig. 5 Effect of the depth of cut (a) on the ratio (F_r/F_c) for different nose radii

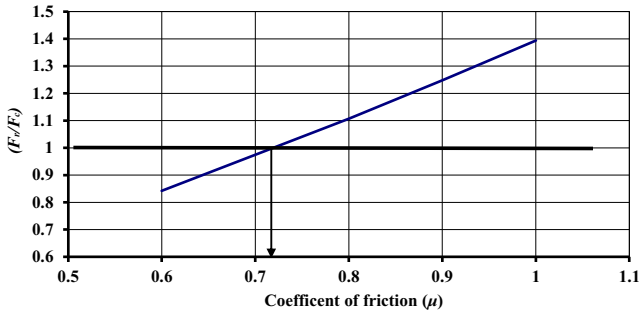

Fig. 6 Increase of (F_r/F_c) at ≥1 caused by the increase of the coefficient of friction (μ) at the tool-chip interface of ≥0.73

4 Verification of the mechanistic model

4.1 Measurement of cutting force components

In this section, the cutting force components (F_c, F_a, F_r) will be studied as a function of the cutting speed (v). First, the annealed HSS workpiece has been machined. Figure 8a illustrates the relationship between the cutting force components and the cutting speed in the range of 40 to 280 m/min (range of continuous chip).

All components attain a peak at v = 40 m/min due to the hot-pressure welding at the chip/tool interface as will be indicated by the peaks of the λ_c and the μ, after which force components drop by about 7 % at v = 60 m/min due to the softening of the workpiece material as a result of the cutting temperature increase. At 275 m/min, all the cutting force components decrease inversely in proportion to the v by a further 10 %.

The increase of the ratio F_r/F_c is a result of the *synergetic* effect of the increase of the effective lead angle as presented in Fig. 7, together with the increase of the μ at the chip-tool interface (Fig. 6). These two phenomena are results of the small ratio ($(a/r) << 1$).

Figure 8b shows the effect of the v on the cutting force components when machining the hardened HSS workpiece. The cutting force components decreasing inversely to the cutting speed is due to the softening effect raising cutting temperature.

Comparing the hardened HSS workpiece cutting force results with the annealed HSS results, it can be noticed that the cutting force components of the hardened HSS are found to be higher by about 50 % than those of the annealed specimens. This can be attributed to the increase of the workpiece hardness and consequently its shear flow stress [35]. The increase of the F_r to be more than F_c is due to the increase of effect of the χ_e as a result of ($a/r << 1$) together with the increase of the chip frictional action on the tool face. The increase of the v from 40 to 150 m/min causes the reduction of all force components by 15 %. The further increase of v from 150 to 280 m/min does

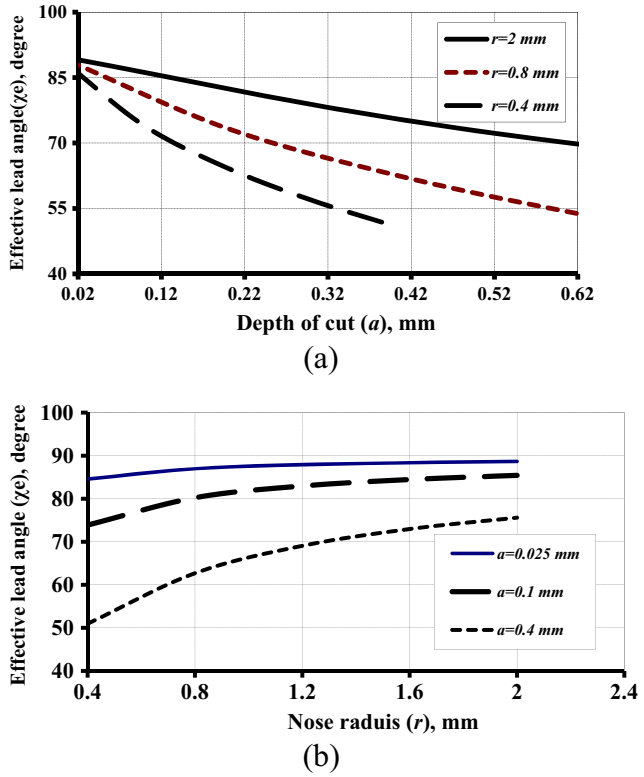

Fig. 7 Effect of the depth of cut (a) on the value of the effective lead angle (χ_e) for different nose radii

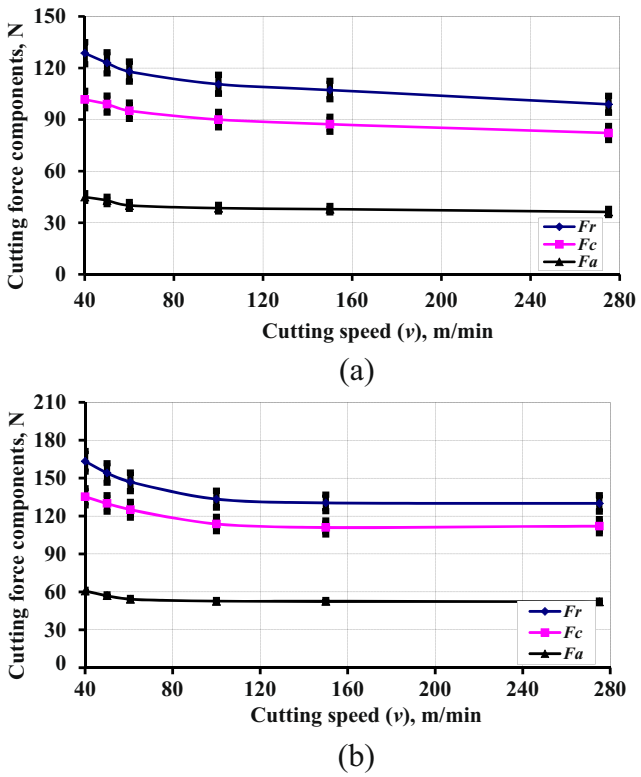

Fig. 8 The relationship between the cutting force components and the cutting speed in the range of 40 to 280 m/min (range of continuous chip)

not cause any significant decrease of the cutting force components.

4.2 Chip compression ratio and coefficient of friction at the tool-chip interface

The λ_c can be used for explaining the behavior of the cutting force and the tool wear mechanisms [36]. Figure 9 shows the chip compression ratio in machining the annealed and hardened HSS at different cutting speeds. A higher chip compression ratio is obtained in machining the annealed HSS than what is obtained in machining the hardened HSS. This can be attributed to the increase of the coefficient of friction at the tool-chip interface due to the more ductile nature of the annealed workpiece with its greater tendency to weld to the tool face.

The μ at the tool chip interface has been calculated for both the annealed and hardened HSS. As illustrated in Fig. 10, the μ has the same behavior indicated by the λ_c presented in Fig. 9. The annealed HSS gives a higher μ than the hardened HSS.

5 Empirical modeling of the cutting force components

The previously presented types of empirical formulae for the cutting force components are based on the following characteristics: specific cutting pressure [37], specific cutting power [38, 39], and specific cutting force [40, 41]. These formulae are not suitable for precision turning. The empirical cutting force relationships to be established in the present work will be based on the specific cutting force. Moreover, an individual formula will be established for each of the cutting force components (F_c, F_a, F_r) and the effect of the tool nose radius and tool flank wear will be considered for conditions of the precision turning operation.

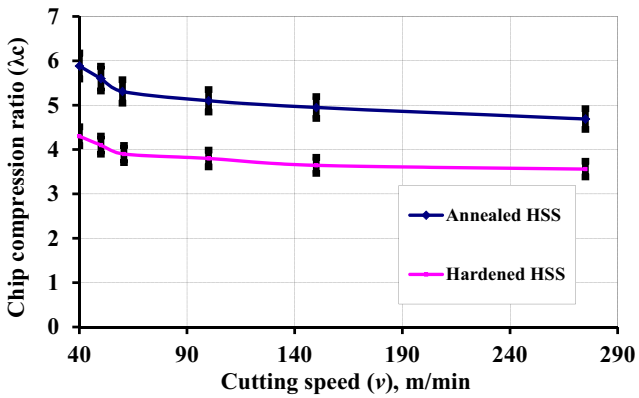

Fig. 9 the chip compression ratio in machining the annealed and hardened HSS at different cutting speeds

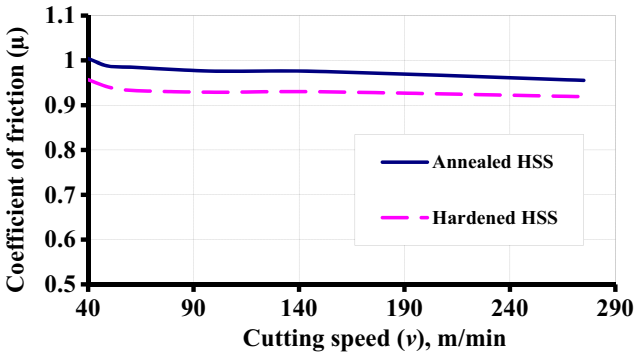

Fig. 10 The coefficient of friction (μ) with the same behavior indicated by the chip compression ratio (λ_c)

5.1 Effect of depth of cut on cutting force components

The effect of the a on the cutting force components for the annealed and hardened HSS is presented in Fig. 11. It is obvious that the increase of the depth of cut increases the values of the three cutting force components due to the corresponding increase of the undeformed chip width (b_1), as ($b_1 \propto \sqrt{a}$). The F_r is the largest affected component, followed by the F_c, while the axial force (F_a) is the least affected one.

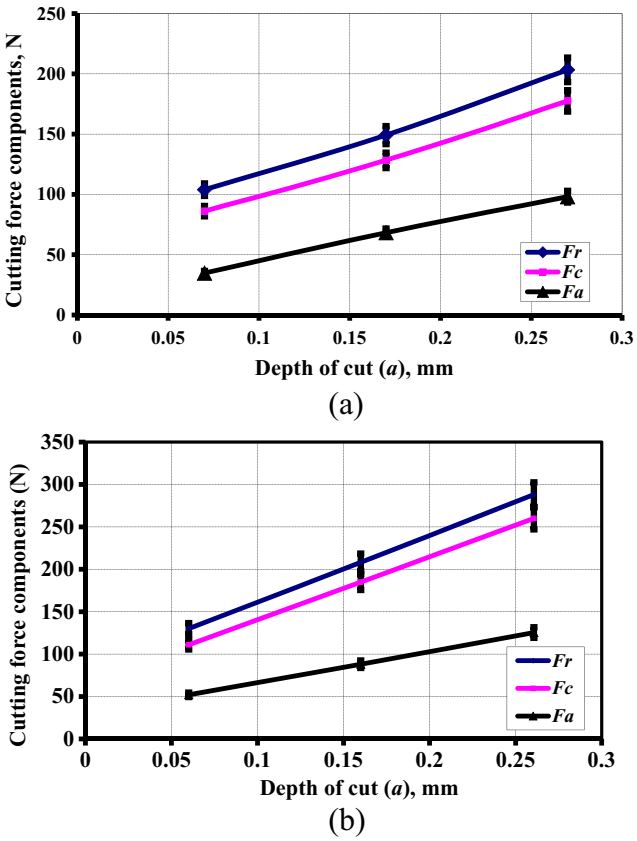

Fig. 11 Effect of the depth of cut (a) on the cutting force components for the annealed and hardened HSS

It can be deduced from Fig. 11 that:

$$F_r, F_c, F_a \propto a^{0.5-0.55} \quad (27)$$

5.2 Effect of feed on cutting force components

Figure 12 shows the effect of the s on the three cutting force components (F_r, F_c, F_a) for the annealed and hardened HSS. Due to the increase of the undeformed chip thickness (h_1) with the s ($h_1 \propto s$), the cutting force components (F_r, F_c, F_a) were also found to increase with the s. However, due to the associated reduction of the coefficient of friction at the tool-chip interface and hence the increase of the shear angle with the s, the cutting force components (F_r, F_c, F_a) increase with the used feed [42].

It can be deduced from Fig. 12 that:

$$F_r, F_c, F_a \propto s^{0.45-0.5} \quad (28)$$

5.3 Effect of tool nose radius on cutting force components

Tool inserts with different nose radii (0.4–1.6 mm) have been used to study the effect of the r on the cutting forces. Figure 13 presents the effect of the r on the cutting force components in machining the annealed and hardened HSS. The F_r and the F_c increase with increasing the r due to its direct effect on the width of cut (b_1), $b_1 \propto \sqrt{2ar}$. F_r increases by 100–115 %, F_c increases by 80–100 %. Since the resultant cutting force approaches the radial direction of the workpiece, the F_a shows only a 10–20 % increase with r.

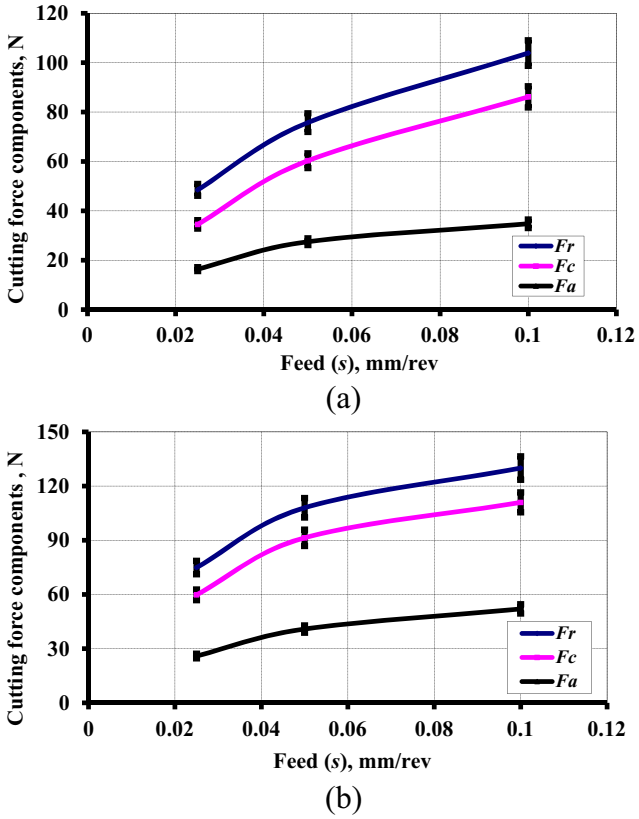

Fig. 12 Effect of feed (s) on the three cutting force components (F_r, F_c, F_a) for the annealed and hardened HSS

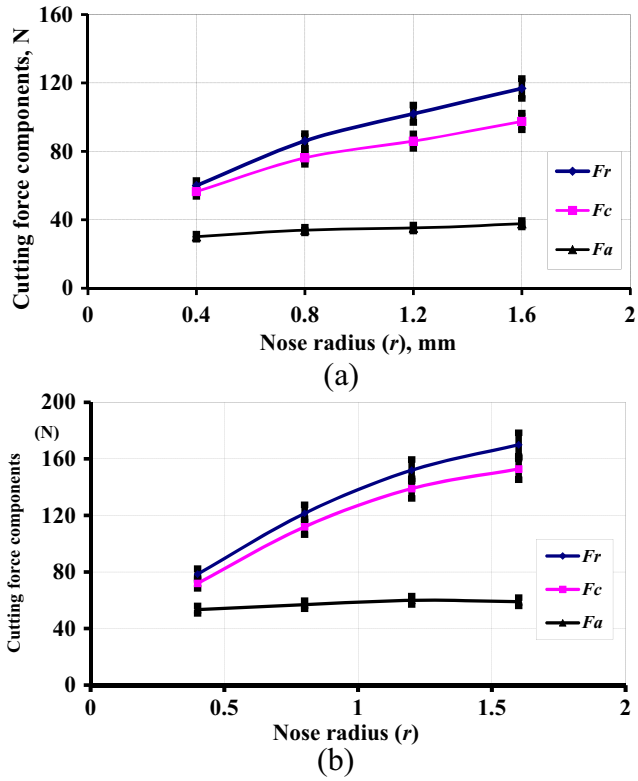

Fig. 13 Effect of the nose radius (r) on the cutting force components in machining the annealed and hardened HSS

It can be deduced from Fig. 13 that:

$$F_r \propto r^{0.5-0.55} \quad (29)$$

$$F_c \propto r^{0.4-0.5} \quad (30)$$

$$F_a \propto r^{0.1-0.15} \quad (31)$$

5.4 Effect of flank wear land width on cutting force components

Figure 14 presents the effect of the tool flank wear width (B) on the cutting force components for both annealed and hardened HSS. Due to flank wear, all the cutting force components increase due to the larger penetration resistance to the tool wedge. A harder workpiece surface exhibits higher resistance than the annealed workpiece surface. At the permissible wear land of 0.2 mm, the radial force of the annealed workpiece increases by 90 %, while the same component increased by

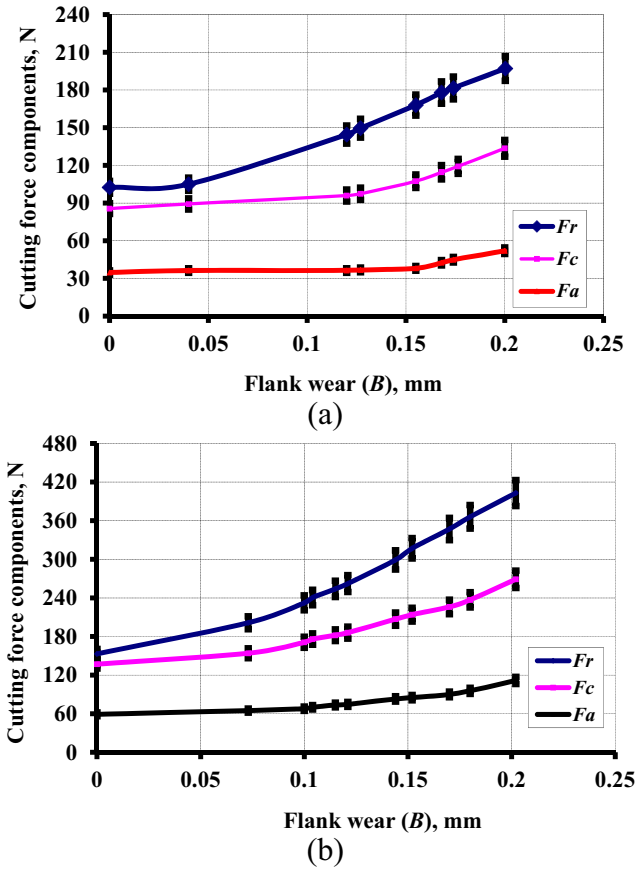

Fig. 14 Effect of the tool flank wear width (B) on the cutting force components for both annealed and hardened HSS

150 % for the hardened one, which is to be viewed as an important consideration in hard precision machining.

Based on Eqs. (27–31) and Fig. 14, the effects of the cutting variables (s, a), r, and the tool flank wear land width (VB) on the cutting force components (F_r, F_c, F_a), the following empirical relationships can be deduced:

Annealed HSS

$$F_r = 1100\, a^{0.5} s^{0.5}\, r^{0.5}\, (1 + 5.5\ \mathrm{VB}) \tag{32}$$

$$F_c = 1160\, a^{0.55} s^{0.55}\, r^{0.4}\, (1 + 3\ \mathrm{VB}) \tag{33}$$

$$F_a = 570\, a^{0.55} s^{0.55}\, r^{0.15}\, (1 + 2\ \mathrm{VB}) \tag{34}$$

Hardened HSS

$$F_r = 1220\, a^{0.5} s^{0.4}\, r^{0.55}\, (1 + 8\ \mathrm{VB}) \tag{35}$$

$$F_c = 1260\, a^{0.55} s^{0.45}\, r^{0.5}\, (1 + 5.5\ \mathrm{VB}) \tag{36}$$

$$F_a = 780\, a^{0.55} s^{0.45}\, r^{0.1}\, (1 + 4.5\ \mathrm{VB}) \tag{37}$$

A maximum deviation, less than 10 % has been detected between the measured and the estimated cutting force values using the given relationships. It has to be mentioned that the presented empirical formulae are only valid in the precision machining range:

Cutting speed, 60 m/min < v < 280 m/min.

Feed, 0.0125 mm/rev <s < 0.1 mm/rev.

Depth of cut, 0.05 mm < a < 0.3 mm.

Nose radius, 0.4 mm < r < 1.6 mm.

Tool flank wear, 0 mm < B < 0.2 mm.

It is obvious that the cutting force components are almost proportional to $a^{0.5}$, $s^{0.5}$, and $r^{0.5}$, as predicted before in Eq. (6), due to the effect of the nose radius in case of a/r < <1.

6 Conclusions

The present study demonstrates a mechanistic model supported by experimental results of precision turning. It was found out that when increasing the r and/or decreasing the a decreases the effective χ and hence increases the χ_e, which directs the cutting force to approach the radial direction, thus increasing the ratio of the F_r to the F_c.

The ratio F_r/F_c becomes ≥1 when $a \le r$. This ratio was found to increase with the increase of r and/or the decrease of the a. The increase of the ratio F_r/F_c to a value greater than (1) is caused by the increase of the μ at the tool-chip interface to be greater than (0.73), which was encountered in the present work. As the chips begins to be continuous, the cutting force components produced from machining the hardened HSS become greater than those produced from machining the annealed HSS due to the higher shear flow stress on the shear plane of the hardened workpiece.

New empirical relationships for predicting the cutting force components in precision turning when (a < <r) have been established. Tool nose radius and flank wear land width were found to have considerable effects on cutting force components. The calculations of the undeformed chip width and thickness have been used to support the empirical equations. The deduced relationships can be used to calculate MFTW system deflection, which is essential to predict the workpiece accuracy, especially in hard precision turning.

References

1. Tonshoff HK, Arendt C, Ben Amor R (2000) Cutting of hardened steel. Annals of the ClRP 49(2):547–566. doi:10.1016/S0007-8506(07)63455-6
2. Campocasso S, Poulachon G, Costes JP, Bissey-Breton S (2014) An innovative experimental study of corner radius effect on cutting forces. CIRP Annals Manufacturing Technology 63:121–124. doi:10.1016/j.cirp.2014.03.076
3. Hashimoto F, Guo YB, Warren AW (2006) Surface integrity difference between hard turned and ground surfaces and its

impact on fatigue life. Annals of the CIRP 55/1:81–84. doi:10.1016/S0007-8506(07)60371-0
4. Jouini N, Revel P, Mazeran PE, Bigerelle M (2013) The ability of precision hard turning to increase rolling contact fatigue life. Tribol Int 59:141–146. doi:10.1016/j.triboint.2012.07.010
5. Afazov SM, Zdebski D, Ratchev SM, Segal J, Liu S (2013) Effects of micro-milling conditions on the cutting forces and process stability. J Mater Process Technol 213:671–684. doi:10.1016/j.jmatprotec.2012.12.001
6. Chen W (2000) Cutting forces and surface finish when machining medium hardness steel using CBN tools. International Journal of Machine Tools & Manufacture 40:455–466. doi:10.1016/S0890-6955(99)00011-5
7. Liu K, Li XP, Rahman M (2003) Characteristics of high speed micro-cutting of tungsten carbide. J Mater Process Technol 140: 352–357. doi:10.1016/S0924-0136(03)00758-1
8. Lima JG, Avila RF, Abrao AM, Faustino M, Paulo DJ (2005) Hard turning: AISI 4340 high strength low alloy steel and AISI D2 cold work tool steel. J Mater Process Technol 169:388–395. doi:10.1016/j.jmatprotec.2005.04.082
9. Huang Y, Liang SY (2003) Cutting forces modeling considering the effect of tool thermal property-application to CBN hard turning. International Journal of Machine Tools & Manufacture 43:307–315. doi:10.1016/S0890-6955(02)00185-2
10. Arrazola PJ, zel T, Umbrello D, Davies M, Jawahir IS (2013) Recent advances in modelling of metal machining processes. CIRP Annals-Manufacturing Technology 62:695–718. doi:10.1016/j.cirp.2013.05.006
11. Bartarya G, Choudhury SK (2012) State of the art in hard turning. International Journal of Machine Tools & Manufacture 53:1–14. doi:10.1016/j.ijmachtools.2011.08.019
12. Aouici H, Yallese MA, Chaoui K, Mabrouki T, Rigal JF (2012) Analysis of surface roughness and cutting force components in hard turning with CBN tool: prediction model and cutting conditions optimization. Measurement 45:344–353. doi:10.1016/j.measurement.2011.11.011
13. Suresh R, Basavarajappa S, Saue GL (2012) Predictive modeling of cutting forces and tool wear in hard turning using response surface methodology. Procedia Engineering 38:73–81. doi:10.1016/j.proeng.2012.06.011
14. Qian L, Hossan MR (2007) Effect on cutting force in turning hardened tool steels with cubic boron nitride inserts. J Mater Process Technol 191:274–278. doi:10.1016/j.jmatprotec.2007.03.022
15. Hosseinkhani K, Ng E (2013) Analysis of the cutting mechanics under the influence of worn tool geometry. Procedia CIRP 8:117–122. doi:10.1016/j.procir.2013.06.075
16. Euan G, Ozturk E, Sims ND (2013) Modeling static and dynamic cutting forces and vibrations for inserted ceramic milling tools. Procedia CIRP 8:564–569. doi:10.1016/j.procir.2013.06.151
17. Agmell M, Ahadi A, Ståhl E (2013) The link between plasticity parameters and process parameters in orthogonal cutting. Procedia CIRP 8:224–229. doi:10.1016/j.procir.2013.06.093
18. Li K, Zhun K, Mei T (2016) A generic instantaneous undeformed chip thickness model for the cutting force modeling in micromilling. International Journal of Machine Tools & Manufacture 105:23–31. doi:10.1016/j.ijmachtools.2016.03.002
19. Zadshakoyan M, Pourmostaghimi V (2013) Genetic equation for the prediction of tool–chip contact length in orthogonal cutting. Eng Appl Artif Intell 26:1725–1730. doi:10.1016/j.engappai.2012.10.016
20. Hosseinkhania K, Ng E (2013) Analysis of the cutting mechanics under the influence of worn tool geometry. Procedia CIRP 8:117–122. doi:10.1016/j.procir.2013.06.075
21. Denkena B, Vehmeyer J, Niederwestberg D, Maaß P (2014) Identification of the specific cutting force for geometrically defined cutting edges and varying cutting conditions. International Journal of Machine Tools & Manufacture 82-83:42–49. doi:10.1016/j.ijmachtools.2014.03.009
22. Zębala W, Kowalczyk R (2015) Estimating the effect of cutting data on surface roughness and cutting force during WC-Co turning with PCD tool using Taguchi design and ANOVA analysis. Int J Adv Manuf Technol 77:2241–2256. doi:10.1007/s00170-014-6382-6
23. Tang L, Cheng Z, Huang J, Gao C, Chang W (2015) Empirical models for cutting forces in finish dry hard turning of hardened tool steel at different hardness levels. Int J Adv Manuf Technol 76:691–703. doi:10.1007/s00170-014-6291-8
24. El Hakim MA, El Awam AM, Sabbagh AS (1983) A computer program for the optimization of the machining variables. Computer & Industrial Engineering 7(4):317–336. doi:10.1016/0360-8352(83)90015-3
25. Kops L, Gould M, Mizrach M (1993) Improved analysis of the workpiece accuracy in turning, based on the emerging diameter. Transaction of the ASME. Journal of Engineering for Industry 115:253–257. doi:10.1115/1.2901657
26. Koenigsbeger F, Tlusty J (1970) Machine tool structures. Pergamon Press, Oxford
27. Jayanti S, Ren D, Erickson E, Usui S, Marusich T, Marusich K, Elanvogan H (2013) Predictive modeling for tool deflection and part distortion of large machined components. Procedia CIRP 12: 37–42. doi:10.1016/j.procir.2013.09.008
28. Smolenicki D, Boos J, Kuster F, Roelofs H, Wyenc CF (2014) In-process measurement of friction coefficient in orthogonal cutting. CIRP annals- manufacturing. Technology 63:97–100. doi:10.1016/j.cirp.2014.03.083
29. El Hakim MA, Abad MD, Abdelhameed MM, Shalaby MA, Veldhuis SC (2011) Wear behavior of some cutting tool materials in hard turning of HSS. Tribol Int 44:1174–1181. doi:10.1016/j.triboint.2011.05.018
30. Khoshdarregi MR, Altintas Y (2015) Generalized modeling of chip geometry and cutting forces in multi-point thread turning. International Journal of Machine Tools& Manufacture 98:21–32. doi:10.1016/j.ijmachtools.2015.08.005
31. Lin B, Wang L, Guo Y, Jiming Y (2016) Modeling of cutting forces in end milling based on oblique cutting analysis. Int J Adv Manuf Technol 84:727–736. doi:10.1007/s00170-015-7724-8
32. Czarnota C, Kone F, Haddag B, Nouari M (2015) A predictive hybrid force modeling in turning: application to stainless steel dry machining with a coated groove tool. Int J Adv Manuf Technol 79: 65–79. doi:10.1007/s00170-015-6801-3
33. Shaw MC (2005) Metal cutting principles. Clarendon Press, Oxford
34. Stephenson DA, Agapiou JS (1997) Metal cutting theory and practice. Marcel Dekker Inc, New York
35. Yan H, Hura J, Shivpuri R (2007) Flow stresses of AISI H13 die steel in hard machining. Mater Des 28:272–277. doi:10.1016/j.matdes.2005.06.017
36. Wright PK, Trent EM (2000) Metal Cutting, 4th edn. Butterworth-Heinemann, Boston
37. DeGarmo's (2007) Materials and processes in manufacturing. John Wiley & Sons Inc, New York
38. Machinery's Handbook (1999) International Press. 25th ed. New York.
39. Kienzle O (1952) Die Bestimmung von Kräften und Leistungen an spanenden Werkzeugen und Werkzeugmaschinen. Z VDI Düsseldorf 94:299–305 German reference
40. Kienzle O (1957) Victor H. Spezifsche Schnittkräfte bei der Metallbearbeitung. Werkstattstechnik und Maschinenbau, Berlin, pp. 224–225 German reference
41. Degner W, Lutze H, Smejkal E (1970) Spanende Fomung. VEB Verlag Technik, Berlin German reference
42. Shalaby, MA (2011) An investigation into high precision turning of some alloy steels. Ph D thesis, Ain Shams University: Cairo, Egypt.